Uncovering remarkable contribution of lasers peak intensity region in holography

Lohit Malik, Alexandre Escarguel, Mayank Kumar, Abhishek Tevatia, Rajpal Singh Sirohi

Uncovering remarkable contribution of lasers peak intensity region in holography

Lohit Malik[1*], Alexandre Escarguel[2], Mayank Kumar[3], Abhishek Tevatia[4] and Rajpal Singh Sirohi[5]

[1]Department of Manufacturing Processes and Automation Engineering, Netaji Subhas University of Technology Delhi, New Delhi – 110 078, India
[2]Aix-Marseille Universit´e, UMR 7345 CNRS, campus Saint J´erome - case 322, av. escadrille Normandie-Niemen, 13397 Marseille cedex 20, France
[3]Department of Mechanical Engineering, Indian Institute of Technology Delhi, New Delhi – 110 016, India
[4]Department of Mechanical Engineering, Netaji Subhas University of Technology Delhi, New Delhi – 110 078, India
[5]Department of Physics, Alabama A & M University, Huntsville, AL 35811, United States

*Email: lohit.malik@gmail.com; lohit.malik@princeton.edu
*Future address: Department of Mechanical and Aerospace Engineering, Princeton University, Princeton, New Jersey – 08540, United States

Abstract

For the scheme of two colour lasers in interference and holography, we uncover remarkable contribution of focusing region (spread) of the peak intensity of superposing laser beams based on the numerical studies and confirm it by mathematical calculations. The pulses having peak intensity for a wider region create better interference pattern, leading to higher modulation depth. Also, such beams having a stronger intensity gradient enhance the range of frequency detuning (difference), which would ease the experimentation in getting better holograms. A comparison of the results achieved with such beams is done with the most commonly used Gaussian beams for the better understanding of the concept for the advancement in holography.

Keywords – Laser beams, peak intensity region, frequency difference, intensity pattern, modulation depth, holography

Introduction

A monochromatic light wave described by $E(\vec{r}, t) = E_0 \cos(\omega t - \vec{k} \cdot \vec{r})$ exists over the whole space for all times, but it does not exist in practice. In practice we have quasi-monochromatic wave, which has limited extent in space, means the coherence length is limited. When we use two waves of slightly different frequencies and superpose them, the obtained interference pattern is not stationary but moving. Since we cannot record such a pattern on a two-dimensional detector, the variation of the time signal is followed at a point, and this type of interferometry is called heterodyne interferometry.

For the better-quality holograms, generally the two superposing lightwaves are coherently obtained from a single light source (laser). When the light is in the form of a pulse of time duration τ or the coherence length of $c\tau$, a hologram can be recorded on a two-dimensional detector so long the path difference between the two superposing pulses remains within the coherence length. It is however experimentally difficult to perform and in the case of femtosecond lasers the difficulty level rises up. Still, the femtosecond holography has validated the recording of static holograms [1, 2]. The femtosecond lasers have proved to be a useful tool in both the transparent and opaque materials with respect to the patterning diffractive elements and in obtaining efficient radiation [3, 4] and wake field in nonlinear media [5, 6].

In a single beam femtosecond laser direct writing technique, a double-layer hologram inside the polymethyl methacrylate sample and a triple layer hologram inside $LiNbO_3$ sample have been constructed [7]. Based on the femtosecond lasers, nonvolatile spectral holography has been conducted in photorefractive Lithium Niobate crystals. With the use of stoichiometric $LiNbO_3:Tb,Fe$, the

two colour hologram multiplexing has been achieved successfully [8]. Apart from these enticing applications, a method based on computational adaptive optics was proposed to rectify the deviations in digital holography [9]. Improvement in quality is always fruitful for imaging techniques. An algorithm was used to improve image resolution based on phase shifting holography [10]. An amplitude-only Fermat-spiral sieve has also been used for holographic imaging that eliminated the limitation at shorter wavelengths [11].

Two femtosecond laser beams with significant frequency difference have been employed for the holography and permanent holographic gratings have been prepared, but the quality could be achieved by keeping the two frequencies very close to each other [12]. As an attempt for the improvement by reducing the null regions, which were developed in such a scheme, we have proposed skewness in the Gaussian pulses [13] for obtaining the better-quality holograms. Also, the femtosecond lasers with zero intensity at their central region have been proved to be better candidates for realizing holograms for large frequency differences [14]. However, now for the first time we show that the spread or focusing region of the peak intensity of lasers is very important for enhancing not only the region of frequency difference but also the modulation depth and intensity pattern and hence, in achieving the better-quality holograms. We make precise numerical studies of the problem and confirm the results and the proposal with the mathematical calculations. Comparative study is done with the most commonly used Gaussian pulses of the lasers in order to prove how important is this proposal for the advancement of the holography technology.

Interference pattern by lasers with wider peak intensity region

A Gaussian pulse profile (temporal) of the laser is described by $E(t) = E_0 e^{-\left(\frac{t}{\tau}\right)^2}$, where E_0 is the amplitude of its electric field and τ is the pulse duration. This profile is shown by the dotted line in figure 1, from which this is clear that the peak of its field (or intensity) stays for a smaller region. However, the expression $E(t) = E_0 e^{-\left(\frac{t}{\tau}\right)^4}$ for another kind of profile is plotted in this figure, which shows that the peak electric field

(intensity) stays for a longer region. This kind of pulse is called as super-Gaussian pulse, where the higher even powers of $\frac{t}{\tau}$, such as 6, 8, 10, etc. (index of the laser), further enlarge this region. A comparison of the two graphs reveals that the peak intensity region for the super-Gaussian beam is much more than that of the Gaussian beam which is relatively pointed. Third graph in this figure is for $E(t) = E_0 \cos h^2\left(0.935\frac{t}{\tau}\right) e^{\frac{-t^2}{\tau^2}}$, which is called $\cosh^2$ profile. This kind of profile is such that its focused region has the same spread as that of the super-Gaussian beam (index 4) but the rise and fall rate of its intensity is appreciably slow. It means the gradient in intensity of the super-Gaussian profile is higher than that of the $\cosh^2$ profile and the Gaussian profile.
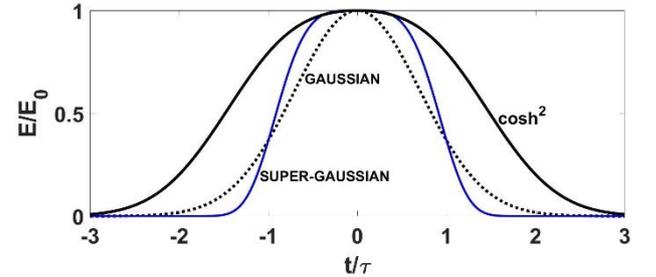

Figure 1. Field profiles for $\cosh^2$ beam, super-Gaussian beam of index 4 and Gaussian beam.

We will make use of these laser beams for obtaining the interference pattern and then the modulation depth from the energy density corresponding to the pattern. The modulation depth that represents the interference modulation efficiency is the main quantity for judging the quality of the holograms obtained. It is one of the most important quantities that manipulates the signal-to-noise ratio of an interferogram and clearly impacts the sensitivity of the spectrometer. This is in general the coefficient of the cosine term in the expression of interference pattern $I = (I_1 + I_2)[1 + M_d \cos \alpha]$ obtained when two coherent beams of intensities I_1 and I_2 and phase difference α are used to interfere. This expression is derived from the resultant intensity $I = I_1 + I_2 + 2(I_1 I_2)^{1/2} \cos\alpha$ and $M_d = (I_{max} - I_{min})/(I_{max} + I_{min}) = 2(I_1 I_2)^{\frac{1}{2}}/(I_1 + I_2)$.

At first we consider two Gaussian beams (n = 2) or super-Gaussian beams (n = 4) having electric fields $E_j(\vec{r}, t) = E_{0j} e^{-\left(\frac{t}{\tau}\right)^n} \cos(\omega_j t - \vec{k_j} \cdot \vec{r})$,

which on superposition yield the following intensity pattern $I(\vec{r}, t) = e^{-\left(\frac{t}{\tau}\right)^n}\left[E_{01}^2 + E_{02}^2 + 2E_{01}E_{02}\cos\left(\delta_\omega t - \overrightarrow{\delta_k}\cdot\vec{r}\right)\right]$. Here $\delta_\omega = \omega_2 - \omega_1$ is the frequency difference (detuning) and $\overrightarrow{\delta_k} = \overrightarrow{k_2} - \overrightarrow{k_1}$ is the wave vector of the pattern, representing the periodicity of the pattern. In order to plot this intensity pattern, we consider the same parameters as used by Odoulov et al. [12] in their experiment, i.e. $E_{01} = E_{02} = 4.38 \times 10^9 V/m$, $\delta_\omega = 12 \times 10^{13} rad/s$, $\delta_k = 4 \times 10^5 /m$ for the lasers having pulse duration of $\tau = 100\, fs$ and $150\, fs$.
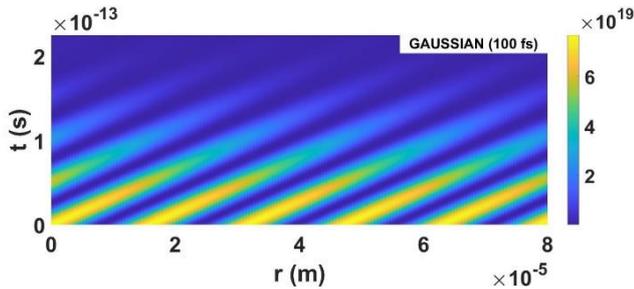
Figure 2. Intensity pattern obtained by Gaussian beams at $\tau = 100\, fs$.
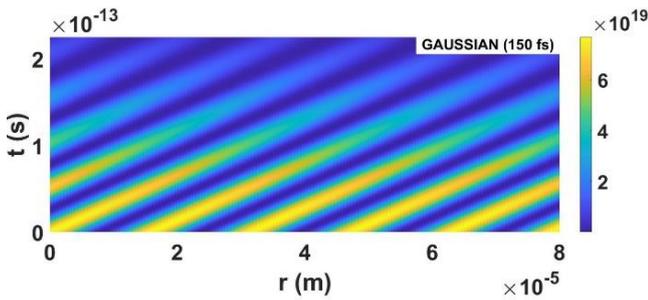
Figure 3. Intensity pattern obtained by Gaussian beams at $\tau = 150\, fs$.
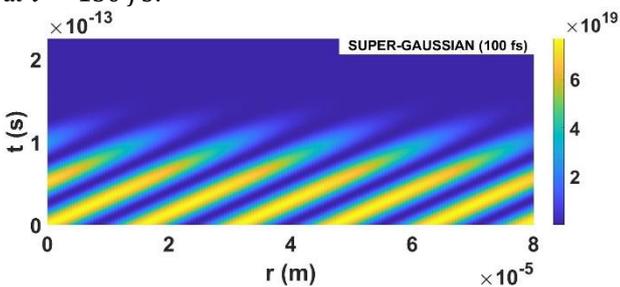
Figure 4. Intensity pattern obtained by super-Gaussian beams at $\tau = 100\, fs$.

Figures 2 and 3 show the intensity patterns in space and time obtained when two Gaussian beams (of either 100 fs or 150 fs pulse duration) superpose, whereas figure 4 shows the pattern for the case of two super-Gaussian beams. Focusing along any one inclined intensity region, one observation in figures 2 and 3 is that the intensity is initially maximum (yellow colour) which gradually falls down (blue colour) and this blue region is laid out till long until the intensity turns zero. Similar observation is made with the super-Gaussian beams, but the rate of fall in the intensity is relatively abruptly to almost zero. It means that the intensity of the pattern in this case is very confined, means the fringes with higher degree of bright dark contrast are obtained with the lasers having wider peak intensity region. Focusing on the maximum intensity regions (bright yellow) in figures 2 - 4, similar observation is made that these regions are found to climb upwards leading to a larger area covered by them as the pulse duration is raised from 100 fs to 150 fs. Since the fringe spacing is determined by $\frac{2\pi}{\delta_k}$, it remains the same in all the cases irrespective of the profile of the laser beams and their pulse duration.

Numerical evaluation of modulation depth

To specifically study the fascinating role of the focusing region, we need to precisely calculate and plot the modulation depth. The formulated intensity pattern is used to calculate the energy density using $E_n(\vec{r}) = \int_{-\infty}^{\infty} I(\vec{r}, t)dt$, which finally leads to the modulation depth (say M_d). Using MATLAB, we could build pertinent programs and accurately solved this problem numerically. The said numerical method integrates the function within the specified limits using the global adaptive quadrature rule and error tolerances. An approximate value I_{approx} of the integral is estimated. This is subtracted from the actual value I to obtain the error estimate as $\varepsilon = \left|I_{approx} - I\right|$. If ε is greater than the desired error tolerance, the interval is divided, and the process is repeated on both the newly created sub-intervals. Finally, the sum of the calculations on each sub-interval is returned.

The numerical calculations reveal that M_d is a function of both τ and δ_ω. For observation we fix $\tau = 75\, fs$ and the graph is plotted between M_d and δ_ω in figure 5. The horizontal line denotes the modulation depth of 0.45, above which holograms obtained are considered to be of appreciable quality. Interestingly, the vertical line dropped from the point of intersection of $M_d = 0.45$ and the

super-Gaussian beam-curve to the X-axis is ahead as compared to the case of the Gaussian beam-curve. Hence, the flexibility for choosing two lasers of significant frequency difference is higher in the case of super-Gaussian beams. This also translates to a higher area under the super-Gaussian beam-curve above M_d of 0.45 relative to the area under the Gaussian beam-curve. Hence, the two-colour holography can be easily applied in view of these results, which was necessary for grating recording to improve the holographic sensitivity of the medium [15].

An additional advantage of using super-Gaussian beams is clear from its secondary peak in figure 5 (and figure 9, later), which rises with the lasers having higher index. This means that it would be possible to generate holograms for a higher frequency difference also, which is impossible in the case of Gaussian beams. Now to meticulously uncover the possible reason for these, we delved deeper and found that all of this is related to the focusing region of the beam. As the region of peak intensity of the Gaussian beams is smaller, it leads to a relatively unconfined intensity pattern (figures 2 and 3) and finally a smaller flexibility or a smaller modulation depth. The modulation depth also vanishes at particular values of δ_ω in the case of super-Gaussian beams. Actually the regions very close to these points correspond to the null regions, as discussed in [13, 14].
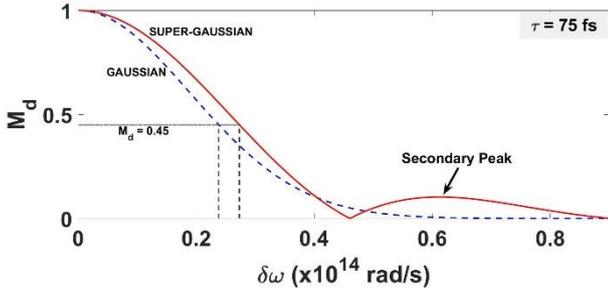
Figure 5. M_d vs δ_ω for Gaussian beams and super-Gaussian beams at $\tau = 75\ fs$.

Comparison and confirmation by mathematical calculations

Now the intriguing question arises: is the above behaviour due to the widening of peak intensity or due to the fast variation in the rate of rise and fall of lasers intensity and our numerical results are correct? To verify this, we obtain analytical solution to the problem by using $\cosh^2$ profile beams that have the same spread of peak intensity (field) as the super-Gaussian beams but smaller intensity gradient. With the said expression of $\cosh^2$ beams having different frequencies and wave numbers, the intensity pattern reads $I(\vec{r}, t) = \cos h^2\left(0.935\frac{t}{\tau}\right)e^{\frac{-t^2}{\tau^2}}[E_{01}^2 + E_{02}^2 + 2E_{01}E_{02}\cos(\delta_\omega t - \overrightarrow{\delta_k}\cdot\vec{r})]$. For the calculation of modulation depth, we find $E_n(\vec{r})$, as

$$E_n(\vec{r}) = (E_{01}^2 + E_{02}^2)\int_{-\infty}^{\infty}\cos h^2\left(0.935\frac{t}{\tau}\right)e^{\frac{-t^2}{\tau^2}}dt + (2E_{01}E_{02})\int_{-\infty}^{\infty}\cos h^2\left(0.935\frac{t}{\tau}\right)e^{\frac{-t^2}{\tau^2}}\cos(\delta_\omega t - \overrightarrow{\delta_k}\cdot\vec{r})\,dt$$

At first we calculate the two integrals separately by assuming $I_{01} = \int_{-\infty}^{\infty}\cos h^2\left(0.935\frac{t}{\tau}\right)e^{\frac{-t^2}{\tau^2}}dt$ and $I_{02} = \int_{-\infty}^{\infty}\cos h^2\left(0.935\frac{t}{\tau}\right)e^{\frac{-t^2}{\tau^2}}\cos(\delta_\omega t - \overrightarrow{\delta_k}\cdot\vec{r})\,dt$. Solving the first integral without limits (say I_1), we get

$$I_1 = \frac{e^{0.87\sqrt{\pi}\tau}\ erf\left(\frac{1000t - 935\tau}{1000\tau}\right)}{8} + \frac{e^{0.87\sqrt{\pi}\tau}\ erf\left(\frac{1000t + 935\tau}{1000\tau}\right)}{8} + \frac{\sqrt{\pi}\tau\ erf\left(\frac{t}{\tau}\right)}{4} + C.I.$$

Putting the limits, we get $I_{01} == \frac{\sqrt{\pi}\tau}{2}(e^{0.87} + 1)$. Similarly, solving the second integral without limits (say I_2), we get

$$I_2 = \frac{e^{-i\overrightarrow{\delta_k}\cdot\vec{r}}}{8}\int\left(e^{\frac{935t}{500\tau}} + 1\right)^2 e^{\left(\frac{-t^2}{\tau^2} - \frac{935t}{500\tau} + i\delta_\omega t\right)}dt$$
$$+ \frac{e^{i\overrightarrow{\delta_k}\cdot\vec{r}}}{8}\int\left(e^{\frac{935t}{500\tau}} + 1\right)^2 e^{\left(\frac{-t^2}{\tau^2} - \frac{935t}{500\tau} - i\delta_\omega t\right)}dt + C.I.$$

Considering $\overrightarrow{\delta_k}\cdot\vec{r} = p$, we solve these integrals. Then putting the limits we obtain

$$I_{02} = \frac{\tau\sqrt{\pi}e^{\frac{-\delta_\omega^2\tau^2}{4}}}{4}\left[e^{0.87}\left\{\cos\left(\frac{1000p + 935\delta_\omega\tau}{1000}\right) + \cos\left(\frac{1000p - 935\delta_\omega\tau}{1000}\right)\right\} + 2\cos p\right]$$
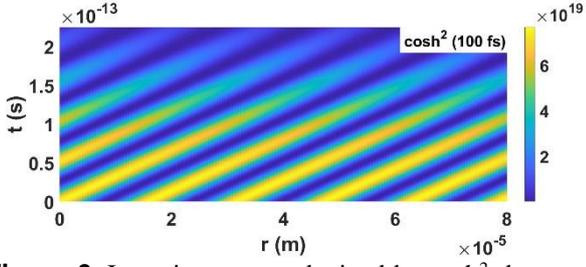
Or

$$I_{02} = \frac{\tau\sqrt{\pi}e^{\frac{-\delta_\omega^2\tau^2}{4}}}{2}[1 + e^{0.87}\cos(0.935\delta_\omega\tau)]\cos(\overrightarrow{\delta_k}\cdot\vec{r})$$

Hence

$$E_n(\vec{r}) = (E_{01}^2 + E_{02}^2)\frac{\sqrt{\pi}\tau}{2}(e^{0.87} + 1) + (2E_{01}E_{02})$$
$$\times\frac{\tau\sqrt{\pi}e^{\frac{-\delta_\omega^2\tau^2}{4}}}{2}[1 + e^{0.87}\cos(0.935\delta_\omega\tau)]\cos(\overrightarrow{\delta_k}\cdot\vec{r})$$

From the above expression, we find the modulation depth, as

$$M_d = \frac{[1 + e^{0.87}\cos(0.935\delta_\omega\tau)]}{(e^{0.87} + 1)}e^{\frac{-\delta_\omega^2\tau^2}{4}} \qquad (1)$$

Figure 6. Intensity pattern obtained by $\cosh^2$ beams at $\tau = 100\,fs$.

The interference pattern obtained by 100 fs $\cosh^2$ beams is shown in figure 6. A comparison of this figure with the earlier ones infers the better confinement of the intensity (yellow colour) in the case of $\cosh^2$ beams than the Gaussian beams but not the super-Gaussian beams. In view of the profiles of $\cosh^2$ and super-Gaussian beams, this can be concluded that the reason for better interference patters / fringes is the rise and fall in the lasers intensity / field and not the region of their peak intensities.

Lasers with stronger intensity gradients produce precise fringes. This observation further strengthens when we compare figures 7 and 8 for the variation of the modulation depth with the pulse duration and frequency difference for $\cosh^2$ and super-Gaussian beams, respectively. Super-Gaussian beams stay the best as they can produce accurate holograms based on the higher modulation depth for broader frequency difference. Such an observation is more evident from figure 9, where the secondary peak in the modulation depth curve is also found to be higher in the case of super-Gaussian beams. Another observation is that the pulses with smaller durations lead to the wider frequency difference for better holograms, consistent to the work discussed in [13] where the role of temporal profile was talked about in detail. The temporal envelopes of the short pulses have also been processed with the help of spectral holography [16]. Recently ultrashort pulses (attosecond signals) have also been considered for realizing double-blind holography, where the reconstruction of missing spectral phases and the characterization of unknown signals could be possible for a finite pulse duration [17]. Since the pulse duration in the present work manipulates the modulation depth, interference pattern and frequency difference (detuning), our proposal might play a vital role in the

reconstruction of missing phases and signal characterization in double-blind holography.
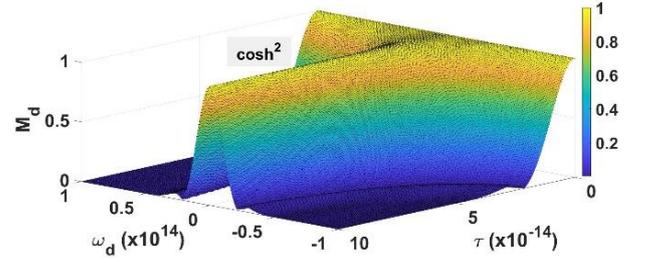

Figure 7. M_d vs δ_ω (rad/s) and τ (s) for $\cosh^2$ beams.
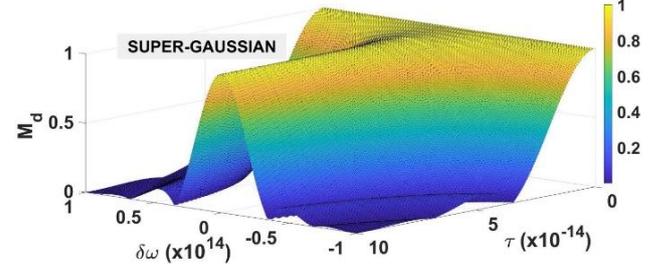
Figure 8. M_d vs δ_ω (rad/s) and τ (s) for super-Gaussian beams.

Above discussion reveals that the better results are obtained for the lasers whose intensity carries stronger gradient. Such lasers have been found to create electron vortices [18] and create plasma channels [19] in addition to their self-focusing and frequency shifting [20]. The point of greater flexibility in frequency difference in the present proposal can be exploited for the application in radiation generation [21].
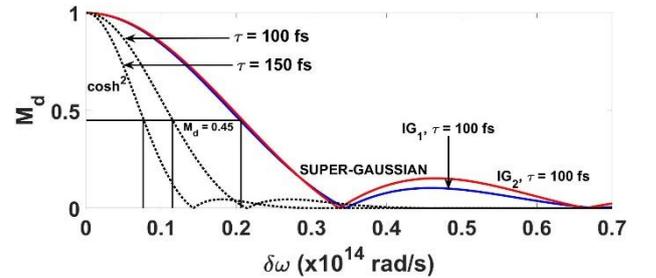
Figure 9. M_d vs δ_ω for $\cosh^2$ beams (dotted lines) and super-Gaussian beams (solid lines). IG stands for intensity gradient, IG$_1$ (n = 4) < IG$_2$ (n = 6).

Finally, we verify the accuracy of our numerical calculations done for the Gaussian and super-Gaussian beams. This is clear that the expression $E(t) = E_0 \cos h^2 \left(0.935 \frac{t}{\tau} \right) e^{\frac{-t^2}{\tau^2}}$ for $\cosh^2$ beams reduces to that of the Gaussian beams if the $\cosh^2$ term reduces to 1. Using this concept in Eq. (1), modulation depth for the Gaussian beams is obtained as $M_d = e^{\frac{-\delta_\omega^2 \tau^2}{4}}$. When we

plotted this for observing its variation with the frequency difference and pulse duration, it exactly matched with the blue dashed line in figure 5 for 75 fs pulse duration. This confirms that our numerical calculations are accurately done.

The occurrence of points corresponding to particular combinations of τ and δ_ω that lead to zero modulation depth in figures 5 and 9 can be explained based on the term $[1 + e^{0.87}\cos(0.935\delta_\omega\tau)]$ in Eq. (1). Here cosine term evolves due to the $\cosh^2$ term appearing in the expression of $\cosh^2$ beam profile. Since $\cosh^2$ term is responsible for the spread of lasers peak intensity region, this is evident that the periodic/oscillating nature of M_d curves (about points $M_d = 0$) is attributed to this intensity spread only. This is further justified when we look at M_d curves for the super-Gaussian beams and the spreading of peak intensity region of these lasers (figure 1). We can also establish a correlation between the interference pattern and the modulation depth by making a comparative study for Gaussian, super-Gaussian and $\cosh^2$ beams. This reveals that the intensity of the pattern in the case of super-Gaussian beams (wider intensity region and higher intensity gradient) is very confined and the fringes with higher degree of bright dark contrast are obtained compared to the cases of Gaussian and $\cosh^2$ beams. Since the highest modulation depth is also obtained in the case of super-Gaussian beams, this is inferred that higher modulation depth is directly related to the confined and better fringe pattern and in this case better holograms can be prepared. On the other hand, this is worth mentioning that the said phenomenon can also be realized with the lasers having spatial profiles in place of the said temporal profiles. In the present case of temporal profile laser beams, the product of "frequency difference δ_ω and pulse length τ in time" is important. However, then the product of "wavelength difference δ_λ and pulse length L in space" will play the same role.

Conclusions

The interference / intensity pattern and the modulation depth were engineered for the lasers having focused intensity (the Gaussian), lasers with wider peak intensity region and stronger intensity gradient (super-Gaussian), and the lasers with wider peak intensity region but weaker intensity gradient ($\cosh^2$) for revealing the remarkable contribution of spreading / widening of the peak intensity in obtaining precise holograms and for advancement of this technique when the two lasers with significant frequency differences are employed. Our numerical and mathematical calculations show that the confined intensity and high-quality fringes of the interference pattern are obtained for the lasers having wider peak intensity region. The situation becomes superior when the intensity gradient of these lasers is raised and their pulse duration is decreased. The modulation depth also assumes higher values for wider frequency differences, when such laser pulses are used. The enhancement in the lasers intensity gradient also leads to the evolution of secondary region of frequency difference for which appreciable value of the modulation depth can be achieved, which would open new regions for exploring the holography technique and further improve the present holographic measurement methods.

Declaration of competing interest
The authors declare that they have no known competing financial interests or personal relationships that could have appeared to influence the work reported in this paper.

References
[1] Abramson N 2011 Motion picture of short pulses. *Nature Photonics.* 5 389

[2] Hsieh HT, Psaltis D, Beyer O, Maxein D, von Korff Schmising C, Buse K and Sturman B 2005 Femtosecond holography in lithium niobate crystals *Opt. Lett.* 30 2233

[3] Malik HK and Malik AK 2011 Tunable and collimated terahertz radiation generation by femtosecond laser pulses *Appl. Phys. Lett.* 99 251101

[4] Malik AK, Malik HK and Kawata S. 2010 Investigations on terahertz radiation generated by two superposed femtosecond laser pulses *J. Appl. Phys.* 107 113105

[5] Dorranian D, Starodubtsev M, Kawakami H, Ito H, Yugami N and Nishida Y 2003 Radiation from high-intensity ultrashort-laser-pulse and gas-jet magnetized plasma interaction *Phys. Rev. E* 68 026409

[6] Dorranian D, Ghoranneviss M, Starodubtsev M, Ito H, Yugami N and Nishida Y 2004 Generation of short pulse radiation from magnetized wake in gas-jet plasma and laser interaction *Phys. Lett. A* 331 77

[7] Sohn IB, Choi HK, Yoo D, Noh YC, Noh J and Ahsan MS 2018 Three-dimensional hologram printing by single beam femtosecond laser direct writing *Appl. Surf. Sci.* 427 396

[8] Lee M, Hatano H, Tanaka S, Yamaji T, Kitamura K and Takekawa S 2002 Two-color hologram multiplexing from the colored state in stoichiometric $LiNbO_3$: Tb, Fe *Appl. Phys. Lett.* 81 4511

[9] Matkivsky VA, Moiseev AA, Gelikonov GV, Shabanov GV, Shilyagin PA Gelikndonov VM 2016 Correction of aberrations in digital holography using the phase gradient autofocus technique *Laser Phys. Lett.* 13 035601

[10] Leihong Z, Dong L, Bei L, Zilan P, Dawei Z and Xiuhua M 2015 Study of key technology of ghost imaging via compressive sensing for a phase object based on phase-shifting digital holography *Laser Phys. Lett.* 12 075202

[11] Zhang X, Zhang J, Zhou S, Liu D and Zhu J 2019 Single-shot phase-shifting digital holography with amplitude-only Fermat-spiral sieves *Laser Phys. Lett.* 16 025002

[12] Odoulov S, Shumelyuk A, Badorreck H, Nolte S, Voit KM and Imlau M 2015 Interference and holography with femtosecond laser pulses of different colours *Nat. Commun.* 6 5866

[13] Malik L and Escarquel A 2018 Role of the temporal profile of femtosecond lasers of two different colours in holography *EPL* 124 64002

[14] Malik L 2020 Dark hollow lasers may be better candidates for holography *Opt. Laser Technol.* 132 106485

[15] Buse K, Adibi A and Psaltis D 1998 Non-volatile holographic storage in doubly doped lithium niobate crystals *Nature* 393 665

[16] Oba K, Sun PC and Fainman Y 1998 Nonvolatile photorefractive spectral holography *Opt. Lett.* 23 915

[17] Pedatzur O, Trabattoni A, Leshem B, Shalmoni H, Castrovilli MC, Galli M, ... and Nadler B 2019 Double-blind holography of attosecond pulses *Nat. Photonics* 13 91

[18] Punia S and Malik HK 2020 Generation and regulation of electron vortices in an underdense plasma by Laguerre-Gaussian laser pulses *Results Phys.* 18 103216.

[19] Dwivedi M and Malik HK 2020 Dynamics of channel formation and self-focusing of q-Gaussian laser pulse *Opt. Lasers Eng.* 129 106070

[20] Malik HK and Devi L 2020 Relativistic self-focusing and frequency shift of super-Gaussian laser beam in plasma *Results Phys.* 17 103070

[21] Malik HK 2020 Generalized treatment of skew-cosh-Gaussian lasers for bifocal terahertz radiation *Phys. Lett. A* 384 126304